RESEARCH ARTICLE

ADVANCED MATERIALS INTERFACES Open Access

www.advmatinterfaces.de

Antimicrobial Multi-Assay Evaluation of (Al-Doped ZnO)-Ag and TiO_2-Ag Nanocoatings: Impact of Direct and Indirect Mechanisms

Damiano Squitieri, Roberta Vitali, Cecilia Bartoleschi, Giulia Lombardini, Margherita Cacaci, Lorenzo Degli Esposti, Camilla Fusacchia, Skerxho Osmani, Luca Gavioli, Francesca Bugli,* and Daniele Valerini**

Infectious diseases caused by pathogenic bacteria, fungi, and viruses pose a global health threat, aggravated by antimicrobial resistance (AMR). This study explores the antimicrobial efficacy of two nanostructured composite coatings —aluminum-doped zinc oxide with silver (AZO-Ag) and titanium dioxide with silver (TiO_2-Ag)— on polyester substrates, against high-priority pathogens: susceptible and resistant *Klebsiella pneumoniae* and *Staphylococcus aureus* bacterial strains, *Candida albicans* clinical fungal strain, and H1N1 influenza virus. A multimodal analytical approach, encompassing SEM, live/dead fluorescence assays, CFU counts, RT-qPCR, and immunofluorescence, supported by ROS quantification, is adopted to evaluate antimicrobial activity and contribution of indirect and direct-contact mechanisms. Both coatings exhibit robust antimicrobial effects especially through indirect mechanisms, with TiO_2-Ag generally more effective than AZO-Ag through indirect interactions while AZO-Ag more effective in some direct-contact scenarios. Bacterial reduction up to ≈99% and viral inactivation of 98% are observed. Cytotoxicity assays reveal some decline in fibroblast viability, underscoring the coatings' potential mainly for non-clinical applications, like packaging or high-touch surfaces. Moreover, the study emphasizes limitations in using single antimicrobial tests and necessity of combining diverse methodologies to comprehensively assess performance and mechanisms of action, finally proposing strategic guidelines for selecting appropriate antimicrobial materials and evaluation techniques tailored to specific application contexts.

1. Introduction

Transmission of infections and diseases associated with pathogenic agents (bacteria, fungi, and viruses) is a crucial threat for worldwide public health, representing one of the major causes of health loss and global deaths, and correspondingly generating enormous economic impact on healthcare costs. About 57% of the worldwide infection-related deceases in 2019 were connected to ≈30 bacterial species susceptible and resistant to antimicrobials, and 5 bacterial species only (including *Staphylococcus aureus* and *Klebsiella pneumoniae*) caused more than a half of these deaths.[1] The antimicrobial resistance (AMR) of pathogenic bacteria is one of the key reasons for such high death rate.[2] The death toll due to AMR in 2021 reached almost 5 million globally, with a number of yearly deceases about doubled from 1990 to 2021 for methicillin-resistant *Staphylococcus aureus* (MRSA) and carbapenems-resistant bacteria, and with a forecasted further increase in the next decades.[3] Indeed, antimicrobial-resistant

D. Squitieri, G. Lombardini, M. Cacaci, F. Bugli
Department of Basic Biotechnological Sciences
Intensive and Perioperative Clinics
Università Cattolica del Sacro Cuore
Rome 00168, Italy
E-mail: francesca.bugli@unicatt.it

The ORCID identification number(s) for the author(s) of this article can be found under https://doi.org/10.1002/admi.202500622

DOI: 10.1002/admi.202500622

R. Vitali, C. Bartoleschi
ENEA – Italian National Agency for New Technologies
Energy and Sustainable Economic Development
Division Biotechnologies BIOTEC-RED
Via Anguillarese 301, Rome 00123, Italy

L. Degli Esposti
Department of Chemistry and Industrial Chemistry
University of Genova
Via Dodecaneso 31, Genova 16146, Italy

C. Fusacchia
Institute of Science
Technology and Sustainability for Ceramics (ISSMC)
National Research Council (CNR)
Via Granarolo 64, Faenza 48018, Italy

Enterobacterales (including carbapenem-resistant *Klebsiella pneumoniae*) and MRSA are included in the critical and high priority pathogens of the Bacterial Priority Pathogens List of the World Health Organization.[4] Besides bacteria, fungi also significantly contribute to mortality and show a growing resistance against antifungal agents.[5] In particular, *Candida albicans* is included in the four most critical fungi of the WHO Fungal Priority Pathogens List,[6] as it is one of the major responsible pathogens for nosocomial infections, commonly forming biofilms on several implantable medical devices.[7] Finally, viral infections also represent a major responsible for human health loss. For example, seasonal influenza viruses are responsible for 3 to 5 million annual cases of severe illness in the world with consequent several hundred thousand deaths.[8,9]

A major path of human infection diffusion is cross-contamination, i.e. the pathogen transfer from a contaminated surface to another and eventually to human beings, taking place in many situations: frequently-touched objects in everyday life (handles, seats, public transports, touch screens, clothes, etc.), clinical environments, surgery rooms and tools, biomedical implants, water/air filtration systems, food & beverage packaging, etc.[10] Surface cleaning treatments by chemical disinfectants can result aggressive for the treated surfaces and potentially harmful for humans, but also represent only a short-term solution since they must be repeated periodically.[11]

An excellent strategy to respond to such threats is the use of effective, safe, and green antimicrobial surface treatments, acting through different mechanisms of actions and being alternative or complementary to common antibiotics and to frequent chemical disinfection. In this regard, inorganic thin films and nanostructured coatings based on metals and metal oxides, as well as on the combination of multiple materials together, are extensively studied as active antimicrobial agents thanks to their efficacy, resistance, and stability.[12–14] In such research field, additional methodologies like combinatorial synthesis approaches or use of machine-learning algorithms can also represent further supporting tools.[15,16] In previous works, we have already tested nanostructured metal and metal oxide coatings, like Ag,[17–19] Al-doped ZnO (briefly denoted as AZO)[20,21] and TiO_2-Ag[22,23] as antibacterial surface treatments against various bacterial species. Those studies employed two different deposition techniques, magnetron sputtering (MS) and supersonic cluster beam deposition (SCBD), capable of tailoring the nanoparticle size and surface morphology of the coatings. Besides a few works reporting some antibacterial tests on Al-doped ZnO films deposited on glass substrates,[24,25] we were the first to report the application of AZO as antibacterial nanostructured coating on flexible bioplastic films (specifically, polylactide),[20,21] followed by a study of antibacterial and antifungal properties of Zn–Al composite oxide films on flexible polyethylene terephthalate,[26] thus representing interesting models for possible usages in food packaging, biomedical tools, flexible electronics, as well as plastic-based objects/surfaces in general. Concerning the combination of metal and metal oxide nanomaterials together, TiO_2-Ag has shown great potential as antibacterial, antifungal and antiviral agent.[27–29] In this regard, we have also already tested the effect of the coating composition against multiple bacterial strains of such metal/metal oxide combination in TiO_2-Ag films[22,23] as well as, for the first time, in antibacterial AZO-Ag nanocoatings,[30] in order to exploit their synergistic action to enhance the antibacterial efficacy and widen the spectrum of action against multiple bacterial species at the same time. However, the influence of direct-contact and non-direct-contact mechanisms of action (hereafter briefly denotes as "direct" and "indirect" mechanisms, respectively) was not unveiled by those works and it is still debated.

Here, we tackle the open issues by studying the antimicrobial effects of AZO-Ag and TiO_2-Ag surface coatings against various critical and high priority pathogens mentioned above, including antibiotic-susceptible and antibiotic-resistant bacterial strains, as well as yeast and virus. Apart from a recent work testing Al-Ag co-doped ZnO in the form of colloidal nanopowders against some bacterial species and *C. albicans* yeast through the zone of inhibition (ZOI) method,[31] to the best of our knowledge, our present work represents the first report about AZO-Ag in the form of nanocoating against antimicrobial resistant (AMR) bacteria and against fungi, and the first examination of AZO or AZO-Ag materials as antiviral agents. Both the examined coatings compositions (AZO-Ag and TiO_2-Ag) are here deposited on polyester plastic, which is normally used in textiles/fabrics, common objects, packaging, biomedical applications, etc. The potential human toxicity of the deposited coatings is also evaluated as a possible discriminating factor to identify their possible fields of application. Additionally, since there exist a multitude of various methods to estimate the antibacterial and antiviral effect of antimicrobial agents,[32–34] here we employ a "multi-assay" approach comparing the results coming from a set of different antimicrobial tests —colony-forming unit (CFU) counting assays, scanning electron microscopy (SEM) observations, and live/dead staining, further supported by the measurement of reactive oxygen species (ROS)— allowing us to put an insight into the antimicrobial mechanisms of action of our coatings and to derive indications about the influence of direct and indirect modes. Only a limited number of studies employed a similar multifaceted approach to evaluate the antimicrobial activity by combining the above-mentioned tests together on coated surfaces. Such studies were typically focused on a

C. Fusacchia
Department of Mathematical
Physical and Computer Sciences
University of Parma
Parco Area delle Scienze 7/A, Parma PR 43124, Italy

S. Osmani, L. Gavioli
Interdisciplinary Laboratories for Advanced Materials Physics (i-LAMP) &
Dipartimento di Matematica e Fisica
Università Cattolica del Sacro Cuore
via della Garzetta 46, Brescia 25131, Italy
E-mail: luca.gavioli@unicatt.it

F. Bugli
Department of Laboratory and Infectious Disease Sciences
Fondazione Policlinico Universitario A. Gemelli IRCCS
Rome 00168, Italy

D. Valerini
ENEA – Italian National Agency for New Technologies
Energy and Sustainable Economic Development
Brindisi research center
S.S. 7 Appia - km 706, Brindisi 72100, Italy
E-mail: daniele.valerini@enea.it

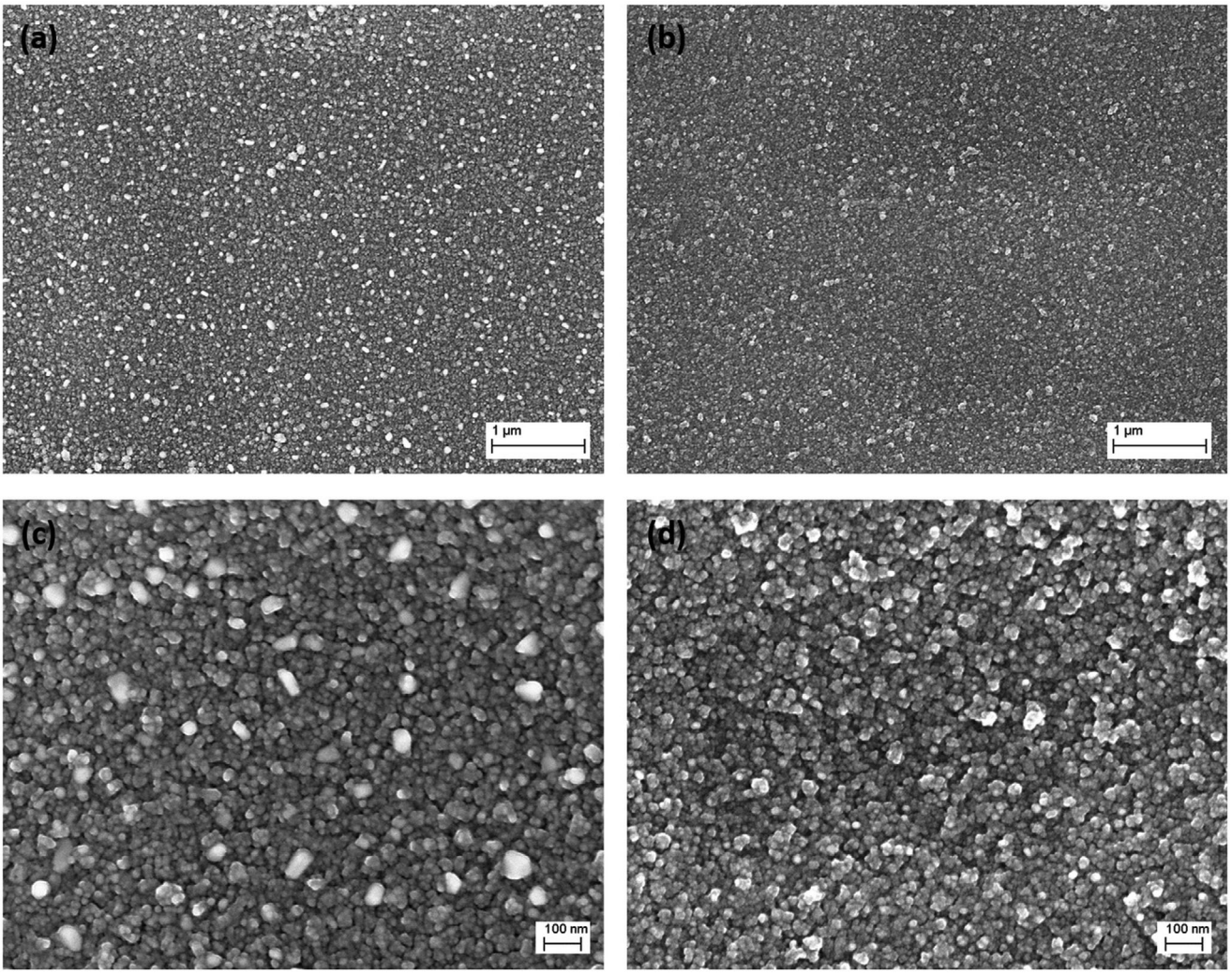

Figure 1. SEM micrographs of AZO-Ag (left column) and TiO_2-Ag (right column) coatings. (a) and (b): lower magnification. (c) and (d): higher magnification.

single bacterial strain or biofilm. To the best of our knowledge, a few works applied this kind of methodology to multiple bacterial species (but not including both susceptible and resistant Gram+ and Gram− bacterial strains in the same analysis),[35,36] or even extending this approach to include fungal pathogens.[37] Hence, here we applied such multi-testing approach on Gram+ and Gram− susceptible and resistant strains and clinical fungal pathogen in the same study, and additionally we analyzed two different metal/metal-oxide coatings (AZO-Ag deposited by MS and TiO_2-Ag deposited by SCBD). As a consequence of the different material and chemico-physical properties of the two coatings, the various antimicrobial mechanisms can have different prominence in the resulting antimicrobial response of the two coatings, which then can be exploited to evidence how the multi-assay approach can give useful indications about the predominance of the different types of mechanisms acting in the two coatings. On such bases, this work strives to provide a critical vision about the suitable materials and proper antimicrobial tests to be preferred depending on the predominant mechanisms of action and on the expected final applications of the coatings, thus offering some general guidelines and advice to their correct selection.

2. Results and Discussion

2.1. Surface Morphology and Composition of As-Deposited Coatings

Field emission-gun scanning electron microscopy (FEG-SEM) analyses (**Figure 1**) evidence that both coatings (AZO-Ag and TiO_2-Ag) present a fine nanostructured surface with high homogeneity, constituted by the mixing and superimposition of Ag and oxide nanoparticles, resulting in grains with a diameter ranging from 10 to 50 nm. In particular, the AZO-Ag surface is characterized by slightly larger grains with respect to the TiO_2-Ag and by the presence of some bigger clusters, as expected by the intrinsic differences of the two deposition processes, as thoroughly explained earlier.[30]

Table 1. Elemental content (weight percentage) in the coatings as evaluated from EDS analyses.

	C wt.%	O wt.%	Zn wt.%	Ti wt.%	Ag wt.%
AZO-Ag	58.5 ± 1.0	28.5 ± 1.5	10.6 ± 0.7	/	2.3 ± 0.3
TiO_2-Ag	68.5 ± 1.0	28.5 ± 1.0	/	1.3 ± 0.2	1.4 ± 0.3

The content of metal elements in the coatings as obtained by energy-dispersive X-ray spectroscopy (EDS) analyses is reported in **Table 1**.

2.2. Antimicrobial Tests

2.2.1. CFU Test for Bacteria and Yeast

Figure 2 reports the antimicrobial activity of coated disks (AZO-Ag and TiO_2-Ag) in comparison to uncoated disks, evaluated through the CFUs count method.

On susceptible strains (Figure 2a,c), the results indicate that both coatings induce a significant reduction of the growth rate for *K. pneumoniae* after 3 h with ≈0.6 Log decrease on AZO-Ag and ≈2 Log decrease on TiO_2-Ag in comparison to the uncoated disk (6.6×10^8 CFU mL^{-1} on uncoated disk versus 1.7×10^8 CFU mL^{-1} on AZO-Ag and 5.2×10^6 CFU mL^{-1} on TiO_2-Ag), while *S. aureus* is significantly reduced after already 1.5 h (2.2×10^7 CFU mL^{-1} on uncoated disk versus 4.6×10^6 CFU mL^{-1} on AZO-Ag and 3.9×10^6 CFU mL^{-1} on TiO_2-Ag) and is subject to a decrease of ≈1 Log on AZO-Ag and 1.7 Log on TiO_2-Ag after 3 h (5.7×10^7 CFU mL^{-1} on uncoated disk versus 4.2×10^6 CFU mL^{-1} on AZO-Ag and 1.1×10^6 CFU mL^{-1} on TiO_2-Ag).

Furthermore, both AZO-Ag and TiO_2-Ag coatings demonstrate good decrease of the growth rate for both *S. aureus* and *K. pneumoniae* resistant strains (Figure 2b,d). At 4.5 h, for resistant *S. aureus*, AZO-Ag induces a 2.5 Log reduction (1.8×10^9 CFU mL^{-1} on uncoated versus 5.6×10^6 CFU mL^{-1} on AZO-Ag), while TiO_2-Ag achieves almost 2 Log reduction (1.8×10^9 CFU mL^{-1} on uncoated versus 2.7×10^7 CFU mL^{-1} on TiO_2-Ag). For resistant *K. pneumoniae*, AZO-Ag shows a 0.3 Log reduction (2.6×10^9 CFU mL^{-1} on uncoated versus 1.2×10^9 CFU mL^{-1} on AZO-Ag), whereas TiO_2-Ag demonstrates a 1.4 Log reduction (2.6×10^9 CFU mL^{-1} on uncoated versus 1.1×10^8 CFU mL^{-1} on TiO_2-Ag,). Finally, tests conducted on *C. albicans* (Figure 2e) demonstrate antifungal activity for both coatings at 4 and 6 h intervals, with the latter showing greater statistical significance. Specifically, after 6 h the measured counts are as follows: 1.8×10^8 CFU mL^{-1} on uncoated disk, 2.6×10^7 CFU mL^{-1} on AZO-Ag, and 1.0×10^7 CFU mL^{-1} on TiO_2-Ag, corresponding to ≈1 Log reduction on both coatings (i.e. 0.8 and 1.2 Log, respectively).

2.2.2. SEM Antimicrobial Evaluation

SEM inspection of the sample surfaces after 4 h contact with microorganisms (bacteria and fungi) reported in **Figure 3** clearly

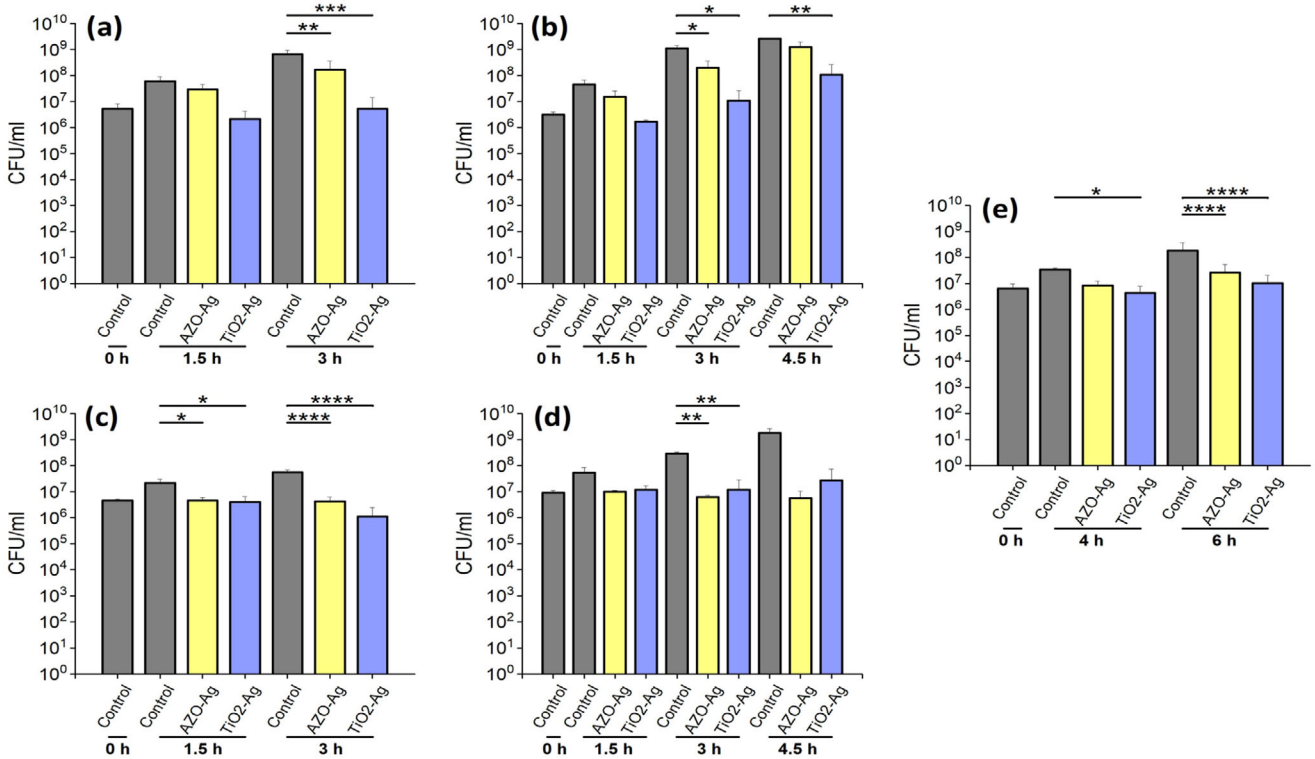

Figure 2. Antibacterial and antifungal effect of AZO-Ag and TiO_2-Ag coatings, evaluated by CFU mL^{-1} count on a) *K. pneumoniae* ATCC 700603 susceptible strain, b) *K. pneumoniae* clinical strain resistant to Carbapenems, c) *S. aureus* ATCC 29213 susceptible strain, d) *S. aureus* clinical strain resistant to Methicillin, and e) *C. albicans* clinical strain. *$p < 0.05$, **$p < 0.01$, ***$p < 0.001$, ****$p < 0.0001$.

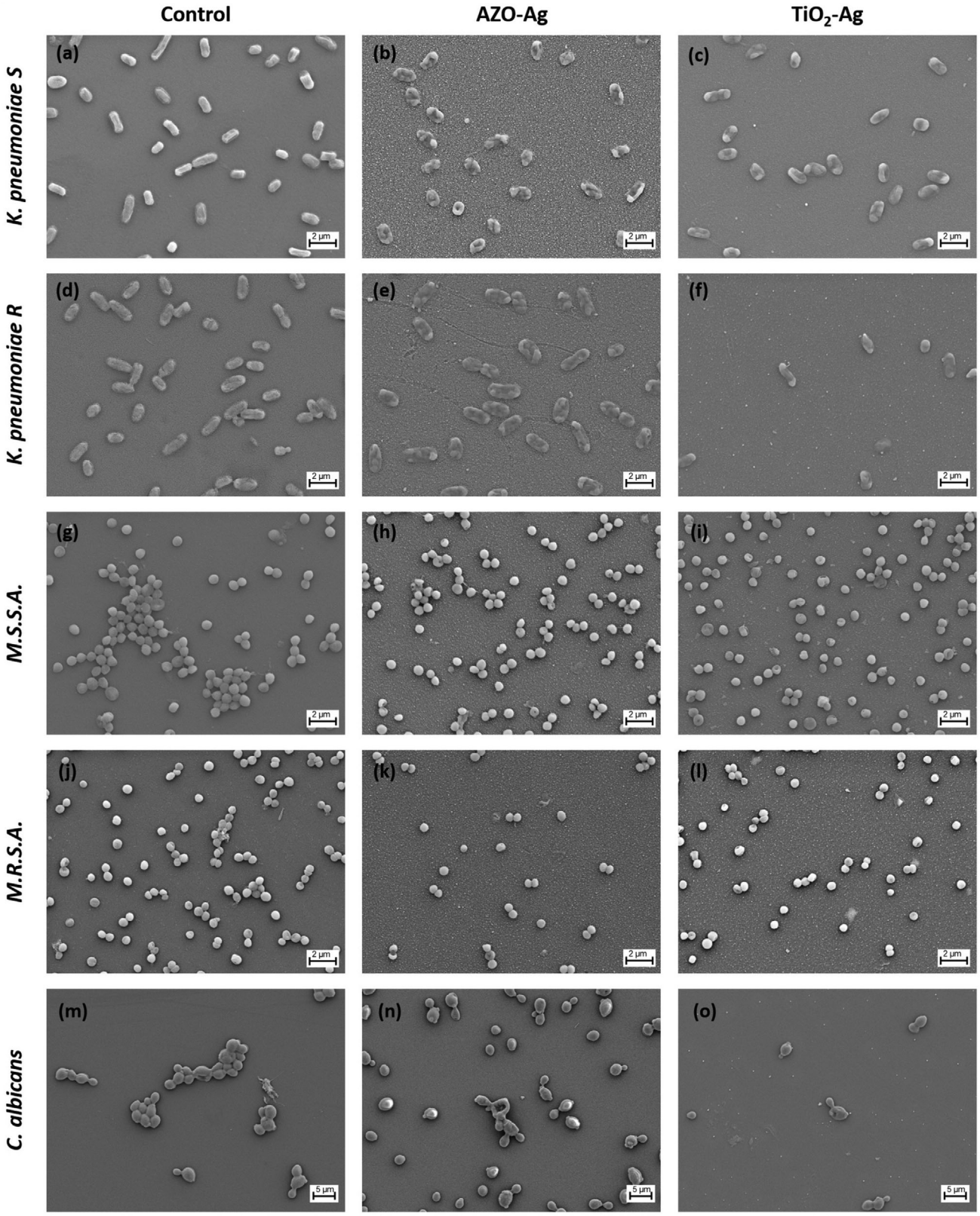

Figure 3. SEM images of sample surfaces (untreated polyester disk controls, AZO-Ag coated disks, and TiO_2-Ag coated disks) after 4 h contact with the tested microorganisms: *K. pneumoniae* susceptible strain (*K. pneumoniae S*), *K. pneumoniae* resistant strain (*K. pneumoniae R*), *S. aureus* susceptible strain (*M.S.S.A.*), *S. aureus* resistant strain (*M.R.S.A.*), and *Candida albicans* (*C. albicans*). Scale bars are equal to 2 µm for bacteria and 5 µm for *C. albicans*.

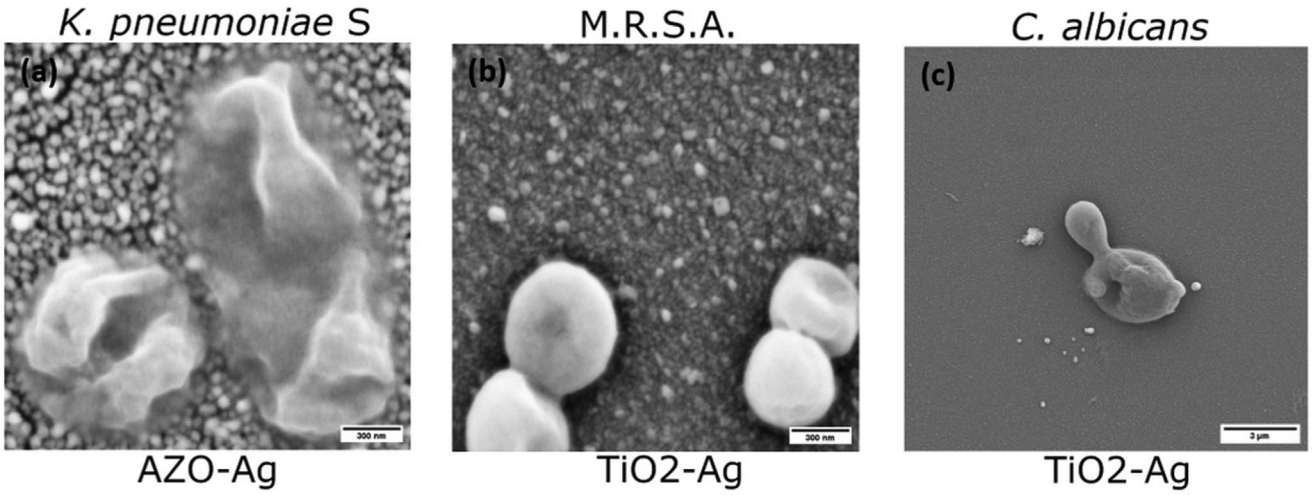

Figure 4. High-magnification SEM micrographs of AZO-Ag coated surface after 4 h contact with *K. pneumoniae* susceptible strain (left), and TiO_2-Ag coated surface after 4 h contact with *S. aureus* resistant strain (center) and *C. albicans* (right). Scale bars are in the bottom right of each micrograph and are equal to 300 nm for bacteria and 3 µm for *C. albicans*.

reveals the occurrence of damages of the microbial cells after contact with both coated surfaces, like cell deformation and cell wall collapse, which are not observed on the adherent cells on the bare plastic surface as visible in the images taken on the untreated control substrates.

Cell damages induced on the coated surfaces are further evidenced in **Figure 4**, showing a representative high-magnification micrograph for each tested species.

The antibiotic-susceptible strain of *K. pneumoniae* in contact with AZO-Ag coated surface (Figure 3b and Figure 4a) shows intensive cell-wall alteration characterized by a wrinkling effect. Methicillin-resistant and susceptible *S. aureus* strains (Figure 3g–l) seem to be generally more resilient to contact-based effects of the coated surfaces than *K. pneumoniae*, with milder cell wall and membrane alterations clearly noticeable in the high magnification images (Figure 4b). These heterogeneous alterations between Gram-negative and Gram-positive bacteria are evident in Figure 4a,b, and they are possibly due to the increased mechanical resistance of Gram-positive cell wall. This behavior is not dependent on the surface coating but seems to be attributable to intrinsic resistance of *Staphyloccocus* cells. Figure 4c also shows evident deformation of budding cells of *Candida albicans* on the coated surfaces, not noticed on the control surface.

In addition to cell deformation and rupture phenomena described above, multicellular agglomeration occurring for *S. aureus* and *C. albicans* on the untreated control surfaces is prevented on the coated surfaces, as visible in Figure 3. These observations are evidence of the antimicrobial actions of the deposited coatings, killing the microbial cells and hindering their reproduction and agglomeration.

2.2.3. Live/Dead Fluorescence Assay for Bacteria and Yeast

Fluorescence micrographs acquired for the different microorganisms on the control polyester disks and on the two coatings are shown in **Figure** 5a–e together with the corresponding quantitative estimation of fluorescence emission from the live/dead assay, plotted in the bottom right panel (Figure 5f–j). This assay is composed of two fluorescent dyes: Syto 9 that can enter viable microbial cells and emits green fluorescence, and Propidium Iodide that can enter only in damaged and dead cells and emits red fluorescent light.

These analyses demonstrate that both coatings conferred good microbiocide action to the plastic surface against all the examined species. The highest effect is observed against *K. pneumoniae* susceptible strain (Figure 5f), where AZO-Ag and TiO_2-Ag coatings induced a cell mortality of (87.61 ± 5.59)% and (78.24 ± 3.26)%, respectively. A similar killing rate (85.45% ± 18.36%) is also observed for the AZO-Ag coating against *S. aureus* susceptible strain (Figure 5h), while TiO_2-Ag shows only a limited action (37.82% ± 9.74%) with a non-significant difference in comparison to growth control (16.15% ± 8.17%). A good antimicrobial action is also noticed against both resistant bacterial species (Figure 5g,i), with a measured percentage of dead cells ≈60–75% (range 58.91–74.19%). Finally, good antifungal action against *C. albicans* (Figure 5j) is detected on TiO_2-Ag coating (killing rate of 78.00% ± 22.43%), whereas AZO-Ag reveals lower action (39.63% ± 2.54%) with a non-significant difference with respect to the uncoated disk.

2.2.4. Quantification of Reactive Oxygen Species (ROS)

After 24 h of contact with the nanostructured surfaces, the production of reactive oxygen species (ROS) was found to be strongly species-dependent compared to the uncoated plastic control surface, as visible in **Figure 6**. *K. pneumoniae* (Figure 6a,b) exhibited a marked increase in oxidative stress when exposed to both AZO-Ag and TiO_2-Ag. Although the increase was slightly higher with TiO_2-Ag, both susceptible and resistant strains showed statistically significant ROS production with both surfaces.

In contrast, *S. aureus* (Figure 6c,d) appeared to be less affected by oxidative stress induced by these surfaces. The measured ROS

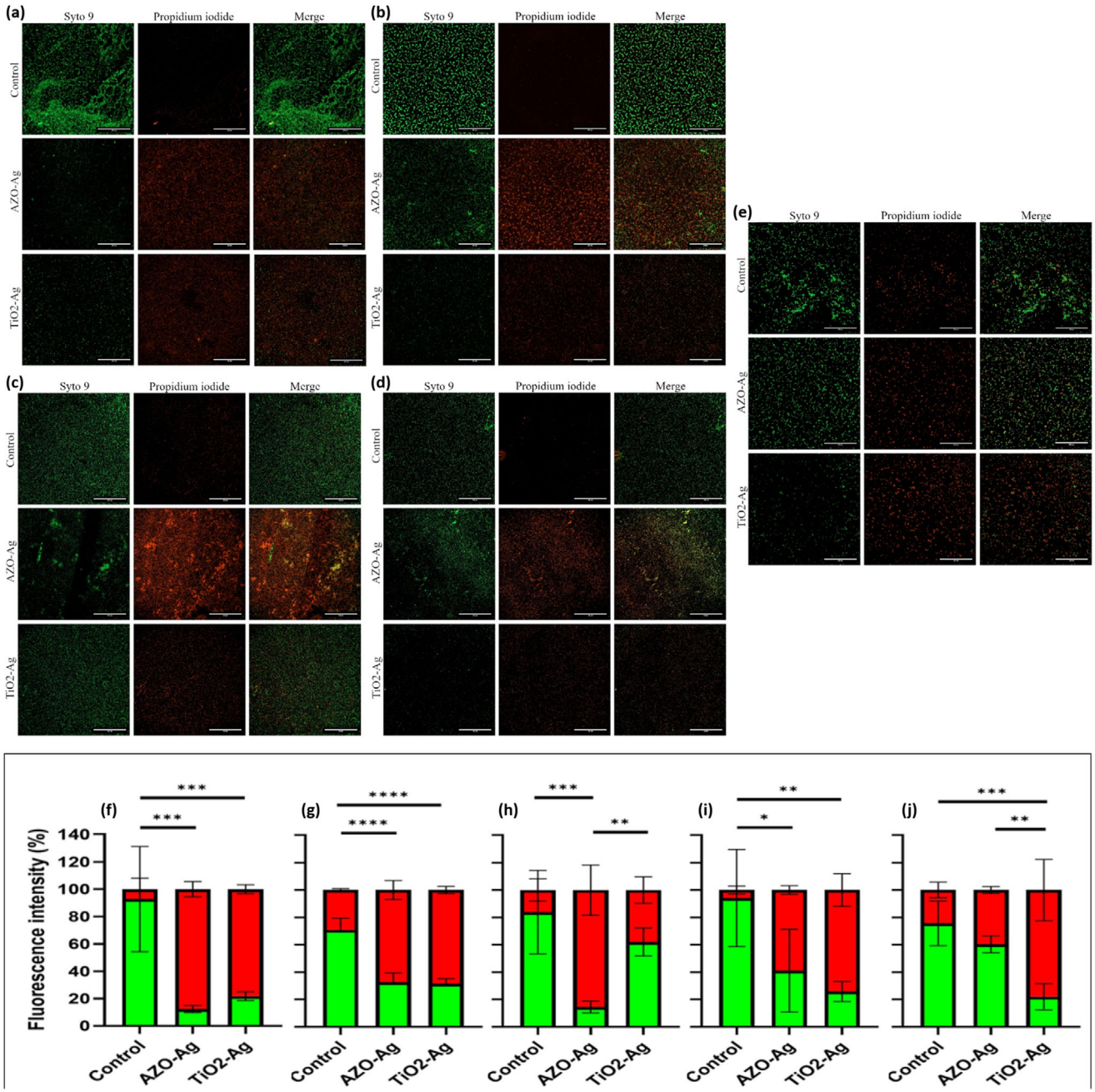

Figure 5. a–e) Images of live/dead fluorescent assays at 20× magnification taken on the uncoated polyester control disks, AZO-Ag coated disks, and TiO_2-Ag coated disks. Fluorescence micrographs, divided by channels in columns, after 4 h contact Images of live/dead fluorescent assays at 20× magnification taken on the uncoated polyester control disks of a) *K. pneumoniae* ATCC 700603 susceptible strain, b) *K. pneumoniae* clinical strain resistant to Carbapenems, c) *S. aureus* ATCC 29213 susceptible strain, d) *S. aureus* clinical strain resistant to Methicillin, and e) *C. albicans* clinical strain. Green (Syto 9) and red (Propidium iodide) fluorescence are associated with live and dead cells, respectively. Scale bar, in the bottom-right corner of each micrograph, is equal to 200 µm. Bottom panel: Quantitative measurements of live and dead cell percentages resulting from fluorescence intensity of f) *K. pneumoniae* susceptible strain, g) *K. pneumoniae* resistant strain, h) *S. aureus* susceptible strain, i) *S. aureus* resistant strain, j) *C. albicans*. Green (Syto 9) and red (Propidium iodide) fluorescence are associated with live and dead cells, respectively. $*p \leq 0.05$, $**p \leq 0.01$, $***p \leq 0.001$, $****p \leq 0.0001$.

levels showed only minor, random fluctuations, none of which reached statistical significance. This suggests that the antimicrobial effect observed against *S. aureus* is likely driven by mechanisms other than ROS induction.

Finally, *C. albicans* (Figure 6e) demonstrated extreme susceptibility to surface-mediated oxidative stress. AZO-Ag exposure led to a fivefold increase in ROS production, while TiO_2-Ag caused an even more pronounced tenfold increase. Both effects were

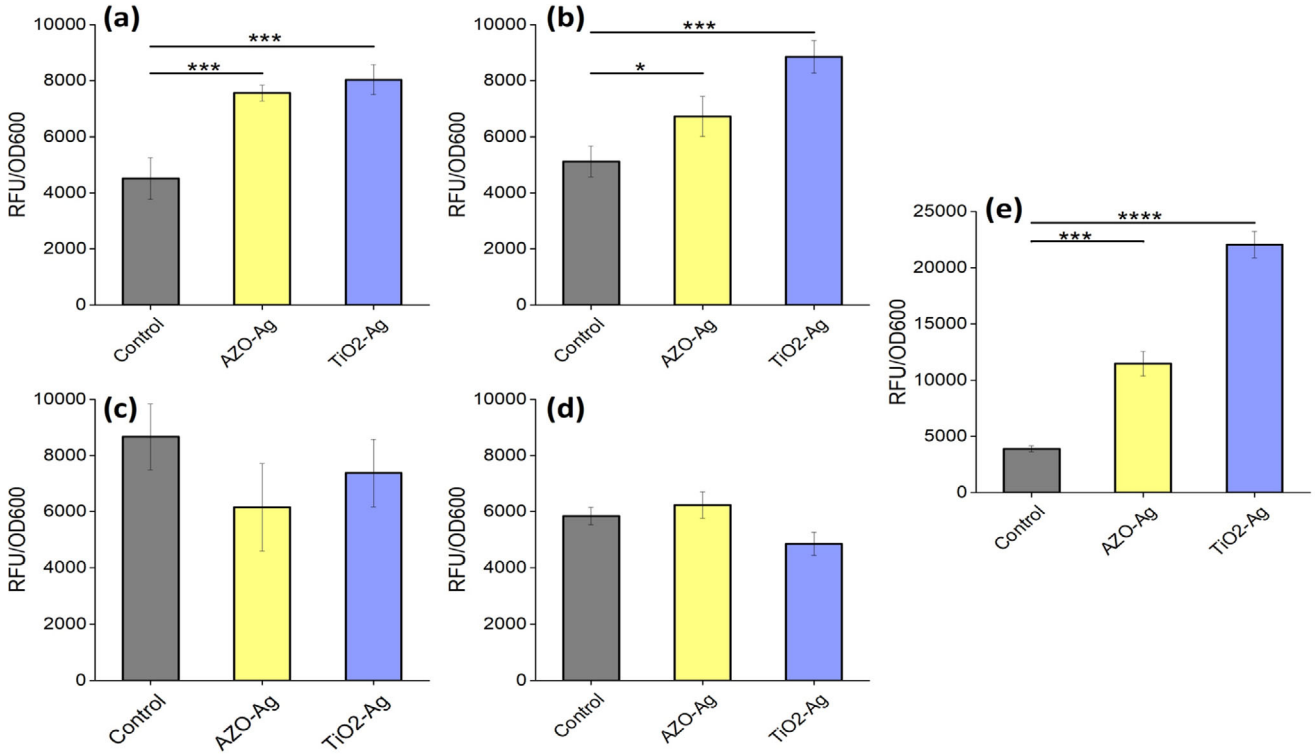

Figure 6. Quantification of reactive oxygen species (ROS) through DCFDA/H2DCFDA on uncoated polyester control disks, AZO-Ag coated disks, and TiO_2-Ag coated disks for a) *K. pneumoniae* ATCC 700603 susceptible strain, b) *K. pneumoniae* clinical strain resistant to Carbapenems, c) *S. aureus* ATCC 29213 susceptible strain, d) *S. aureus* clinical strain resistant to Methicillin, and e) *C. albicans* clinical strain.

statistically significant, confirming the strong oxidative impact of the nanostructured surfaces on this fungal species.

2.2.5. Real-Time PCR and Immunofluorescence for Virus

To assess the antiviral activity of the coated surfaces in preventing the viral infection of MDCK-STAT1 cell line, a real-time polymerase chain reaction (PCR) was conducted.

As evidenced in **Figure** 7a, both coated surfaces significantly reduce the viral load (comparable to matrix gene expression) when compared to bare plastic surfaces, as the values measured for the coated surfaces are ≈2–3% with respect to the uncoated surface, i.e. almost 2 Log_{10} of viral reduction. This result highlights an important antiviral feature of the two coatings: the effectiveness of slowing down the potential spreading of respiratory viruses toward abiotic surfaces.

Figure 7b shows the immunofluorescent assay conducted with a primary antibody directed toward type-1 hemagglutinin (H) protein of the viral envelope. Secondary antibody is linked to FITC fluorescent dye, and a nuclear counterstaining with DAPI was performed. The obtained micrographs show a lower total green fluorescence emission for both AZO-Ag and TiO_2-Ag surfaces, with higher viral inhibition on AZO-Ag coated surfaces compared to TiO_2-Ag and uncoated polyester, and the cellular morphologies in infected monolayers seem to be altered for all tested samples. Both surfaces are not able to completely inhibit the viral capabilities to infect MDCK-STAT1 cells and to avoid monolayer's morphology alterations.

2.3. Discussion on Antimicrobial Mechanisms and Different Experimental Methods

The values of microbial reduction *R(%)* calculated through Equation (1) and antimicrobial activity *A* calculated through Equation (2), resulting from the different antimicrobial methods as detailed in the Experimental Section (paragraph Antimicrobial Tests - *Assessment of Microbial Reduction and Antimicrobial Activity*), are reported in **Table** 2.

The different responses observed against the various tested microorganisms are connected to the specific characteristics of each strain,[12] like e.g.: the essential cell structure (bacterial prokaryotic cell, fungal eukaryotic cell, or virions with a protein shell (capsid) and sometimes an additional lipid envelope); different cell wall features (composition, thickness, presence of multiple layers) between fungi and bacteria, as well as between Gram-positive and Gram-negative bacteria; tendency to form multicellular aggregates in some bacterial and fungal species. Consequently, the same antimicrobial agent can act differently in striking and inactivating or destroying the pathogenic microorganisms depending on each strain considered. Despite that, both coatings (AZO-Ag and TiO_2-Ag) demonstrated a significant efficacy against all the tested pathogens, with an overall microbial reduction ranging from ≈75% up to practically 100% in most cases,

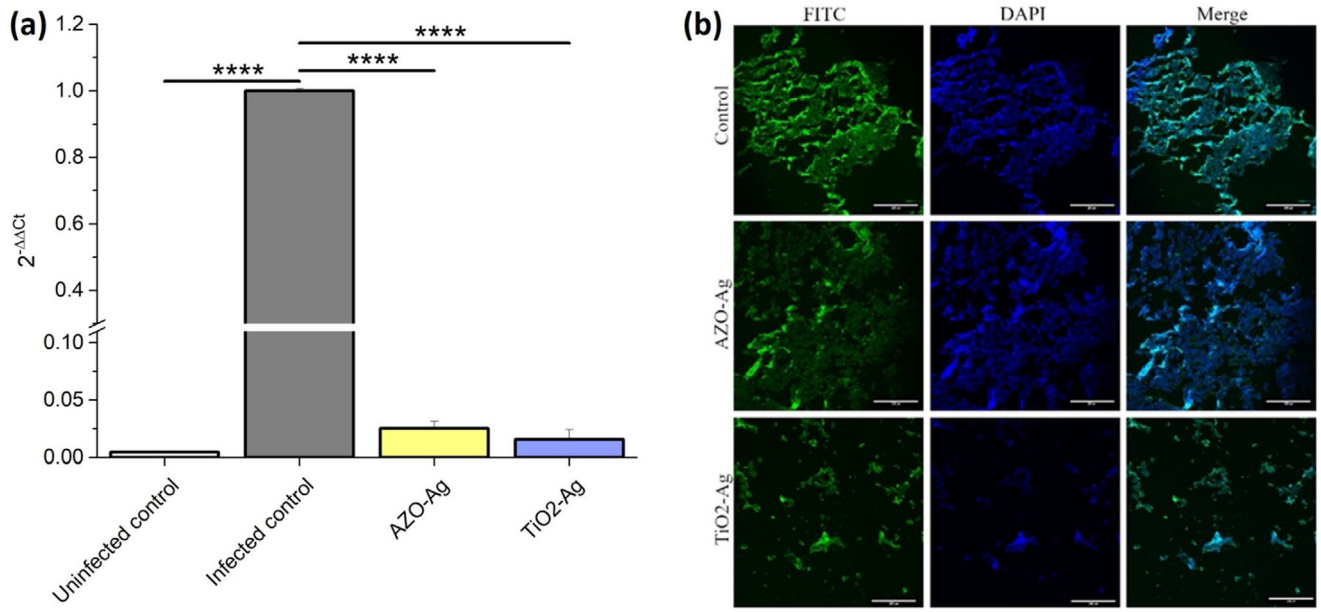

Figure 7. a) Viral load of H1N1 on infected MDCK-SIAT1 cells after direct contact with coated and uncoated surfaces (infected control). An uninfected control was carried out to assess absence of viral RNA in used medium. The viral load is expressed as $2^{-\Delta\Delta Ct}$ expression of retrotranscribed RNA of M matrix protein of H1N1 virus. ****$p < 0.0001$. b) Immunofluorescence images of MDCK-STAT1 cells infected with Influenza H1N1, taken at 20x magnification. Cell monolayers were infected with pre-treated virus incubated for 2 h on coated (AZO-Ag, TiO_2-Ag) and uncoated (polyester control disks) surfaces. Scale bar, in the bottom-right corner of each micrograph, is equal to 200 µm.

reaching a very good antimicrobial activity value *A* of ≈2 in the best situations. The activity here observed for TiO_2-Ag coating on the plastic surface agrees with the known antimicrobial efficacy against sensitive and resistant bacterial strains, fungi, and viruses, widely reported in the literature for TiO_2-Ag nanocomposite coatings on various other kinds of substrates like glass, steel, etc.[22,23,27–29] Looking at the less-explored AZO-Ag coating, the data acquired in the present work confirm the antibacterial effect already observed for AZO-Ag coated plastic surfaces against sensitive strains[30] and further demonstrate its good efficacy also against antibiotic-resistant bacterial strains. Additionally, while antifungal action against *C. albicans* was observed for colloidal Al-Ag co-doped ZnO nanoparticles,[31] here we demonstrate good antifungal effect through CFU tests for AZO-Ag as surface coatings too, together with strong antiviral action.

The experimental data evidenced some differences depending on the strain examined and on the method used to quantify the antimicrobial activity, whose discussion requires an insight into the antimicrobial mechanisms prevailing in each experimental method. It is known that the biocidal effects caused

Table 2. Coating efficiency against sensitive (S) and resistant (R) bacterial strains, yeast (*C. albicans*), and virus (H1N1 influenza) resulting from live/dead fluorescence assays, CFU tests and real-time PCR measurements. *R(%)* represents the microbial reduction detected on coatings versus control calculated using Equation (1), while *A* represents the antimicrobial activity of the coatings calculated using Equation (2).

		AZO-Ag		TiO_2-Ag	
		R(%)	*A*	*R(%)*	*A*
Live/dead fluorescence assay	***K. pneumoniae S***	(87 ± 6)%	0.89	(77 ± 9)%	0.65
	S. aureus S	(81 ± 8)%	0.73	(26 ± 16)%	0.13
	K. pneumoniae R	(54 ± 13)%	0.34	(55 ± 9)%	0.35
	S. aureus R	(56 ± 21)%	0.36	(73 ± 13)%	0.56
	C. albicans	(20 ± 11)%	0.10	(71 ± 15)%	0.54
CFU test	***K. pneumoniae S***	(75 ± 20)%	0.60	(99 ± 1)%	2.11
	S. aureus S	(93 ± 4)%	1.13	(98 ± 2)%	1.71
	K. pneumoniae R	(82 ± 15)%	0.74	(99 ± 1)%	2.02
	S. aureus R	(98 ± 1)%	1.68	(96 ± 5)%	1.40
	C. albicans	(75 ± 10)%	0.61	(87 ± 10)%	0.90
Real-time PCR	**Influenza virus H1N1**	(97 ± 1)%	1.60	(98 ± 1)%	1.81

by inorganic nanostructured materials are generated by several concurrent mechanisms[13,38] that we can group into two main categories:

1) *Direct mechanisms*: mechanical abrasion of the microbes with the nanometric features of the coating surfaces, direct transfer of ions and nanoparticles between the coating and the microbes touching the surface, generation of reactive oxygen species (ROS) at the contact points of microbes and coatings. These mechanisms can prevail against the sessile microbial population formed on the sample surfaces.
2) *Indirect mechanisms*: transfer of nanoparticles, ions, or ROS from the coating to the microbes through the surrounding medium. These mechanisms are predominant against the planktonic microbial population floating in the medium.

Such processes induce a series of combined effects on the bacterial, fungal or viral constituent units, like damage and rupture of the cell wall or virus shell/envelope, leakage of cellular content, disruption of cell metabolism, damage of the microbial genetic material (DNA, RNA), etc., thus leading to the inhibition of microbial growth/reproduction and eventually death of the microbial units.[13,38]

Due to the experimental peculiarities of each antimicrobial test, it is evident how different testing methods can be influenced to different extents by the combination of the multiple direct and indirect processes occurring during the interaction between the coatings and the pathogens. As a consequence, extended information should be derived by gathering results coming from multiple tests. Direct mechanisms are expected to play a more significant role in live/dead assay technique with respect to the CFU count method. Indeed, in live/dead tests the microbes are placed in a non-nutrient solution so that they are forced to adhere to the specimen surface, where then they undergo damages through direct contact with the surface. These effects were clearly noticed in SEM images acquired after the tests (Figures 3 and 4), where microbial cell deformation and breakage is evident. On the contrary, during the CFU count experiments the microbes are placed in a nutrient culture medium where they can grow in their planktonic state, hence indirect mechanisms conveyed through the medium can prevail. Consequently, the higher microbial reduction (i.e. better antimicrobial activity) usually detected by the CFU method versus the live/dead test on both coatings can indicate that indirect mechanisms are predominant over the direct contact ones for both our coatings. Additionally, the higher antimicrobial effect observed for AZO-Ag versus TiO_2-Ag on susceptible strains in live/dead fluorescence tests and for TiO_2-Ag in CFU experiments suggest that direct-contact mechanisms are more effective in AZO-Ag against the tested susceptible strains while indirect mechanisms are generally more effective in TiO_2-Ag than in AZO-Ag. Analogously, antifungal effect against *C. albicans* through indirect action in CFU tests looks slightly better in TiO_2-Ag than in AZO-Ag, in conjunction with direct-contact damage effects already evidenced in SEM inspections (Figures 3 and 4). In this regard, it is also important to note that a method capable of detecting primarily the antimicrobial action on the sessile form, like the live/dead assay, could be particularly useful when dealing with biofilms too.

Additional understanding about the antibacterial/antifungal mechanisms can be derived from the analysis of ROS measurements. Our results demonstrate that the induction of oxidative stress by nanostructured AZO-Ag and TiO_2-Ag coated surfaces is highly species-dependent. *K. pneumoniae* and *C. albicans* both displayed significant increases in ROS production, while *S. aureus* showed no statistically significant changes. The strong oxidative response in *K. pneumoniae* suggests that Gram-negative bacteria are more vulnerable to redox imbalance, possibly due to their outer membrane facilitating ion interactions and their relatively weaker antioxidant defenses. Conversely, the lack of ROS increase in *S. aureus* points to its efficient oxidative stress management, likely supported by its thick peptidoglycan layer and robust enzymatic detoxification systems.[39–41] This indicates that the antimicrobial activity observed against *S. aureus* may rely on alternative, non-oxidative mechanisms such as membrane disruption or toxicity induced by nanoparticles and metal ions released by the coating surfaces. The most striking effect was observed in *C. albicans*, which exhibited extreme susceptibility to ROS, particularly with TiO_2-Ag surfaces. The fungal cell's extensive membrane system and limited antioxidant defenses likely account for this pronounced vulnerability.

Finally, dealing with the antiviral action of the coatings, it must be noticed that this aspect is more complex and less explored than their antibacterial action, also due to higher complexity of the experimental procedures and greater safety precautions needed. For these reasons, it is somehow harder to carefully differentiate about the influence of direct and indirect mechanisms of actions in this case. However, it is important to evidence the great virucide action against the H1N1 influenza virus observed for both coatings, being capable to induce a 97–98% viral load reduction (antiviral activity value *A* close to 2) with respect to the uncoated plastic surface, as visible in Figure 7a and Table 2. Nevertheless, such ability to drastically cut down the virus presence on the treated surfaces cannot exclude completely the possibility for the residual virus to provoke some infection of the mammalian cells, as derived from the immunofluorescence analyses reported in Figure 7b.

Considering the observations above, some fundamental remarks can be drawn:

1) Since the different experimental methods for evaluating the antimicrobial activity of a material can be influenced to a more extent by an antimicrobial mechanism rather than another, it is important to be aware that the use of a single method can provide only a partial indication of the efficacy of a material, giving rise to results that are dependent on the main mechanisms involved in the method. Therefore, whenever possible, a combination of multiple methods should be recommended to obtain a more comprehensive view of the coating efficacy by cross-checking the results achieved through each method.
2) The choice of a specific antimicrobial test rather than another should be also made in view of the expected final application of the examined materials. For example, if the material is intended to act mainly by direct contact with a contaminated surface (e.g., frequently-touched surfaces/objects, textiles, packaging at direct contact with food, etc.) then a test method influenced predominantly by direct contact mechanisms is advisable. On the contrary, a test method affected principally by

indirect (non-contact) action should be recommended when the antimicrobial surface is intended to act mostly at non-direct-contact with the microbes (e.g., food & beverage packaging with liquid content, water filtration/purification systems, etc.). Finally, the use of multiple test methods and the cross-check of their results could be pivotal when the material has to be used on components where both mechanisms (direct-contact and indirect action) can be relevant, like medical devices for human body, such as cannulas, dental implants, prosthesis, pacemakers, other implantable devices, wound healing systems, etc.

3) At the same time, the choice of a suitable material should be also made depending on its most effective antimicrobial mechanisms in view of the intended final application. If the surface is expected to act significantly by both direct and indirect modes, then the choice should be focused to a coating with adequate effectiveness through both routes, or to the combination of multiple materials and adjustment of the surface morphology to optimize both effects.
4) Finally, since each microbial species (Gram+ or Gram- bacterial strains, susceptible or resistant strains, fungi, and viruses) can be affected to different extents by direct or indirect antimicrobial action, a suitable coating material should be chosen depending on the microbial typologies expected to be involved in the final use. Otherwise, a combination of selected multiple materials acting through different predominant mechanisms should be adopted to increase the antimicrobial action and to widen the spectrum of action against different microbe types.

2.4. Cytotoxicity on Mammalian Cells

Potential cytotoxic effect of AZO-Ag and TiO_2-Ag was assayed on murine embryonic fibroblasts (MEFs). Exposing MEFs to coated disks for 24 h reduces cell viability on both coated surfaces with respect to the uncoated polyester control disk. In particular, AZO-Ag treatment induces a cell loss of 95%, and TiO_2-Ag a reduction of 70% (**Figure 8**).

The possible toxicity of metal and metal oxide materials, especially in their nanoparticle form, to humans, animals and the environment is an extremely debated and controversial aspect, with results that are often conflicting, since they are strongly dependent on the combination of a multitude of physicochemical factors, like materials composition, size, shape, crystallinity, surface morphology, surface chemical reactivity, surface charge, particle agglomeration, dose, solubility, catalytic activity, etc., as well as external/environmental factors, like the considered cell types/lines and the way of contact (inhalation, ingestion, skin absorption).[42,43] In particular, nano-silver toxicity is a great concern,[44] and sometimes Ag nanoparticles have been found more toxic than metal oxide ones.[45,46] In a previous work,[21] we have already found negligible toxicity of the single AZO oxide coating (i.e. without the addition of Ag) toward certain human cell lines, as also confirmed in other works,[47,48] hence we assume that the high toxicity observed here can be mainly ascribed to the presence of Ag in the mixed coating composition. This assumption is also supported by the higher content of Ag detected in EDS measurements on the AZO-Ag coating (Table 1), which is indeed resulting in higher cytotoxicity compared to TiO_2-Ag.

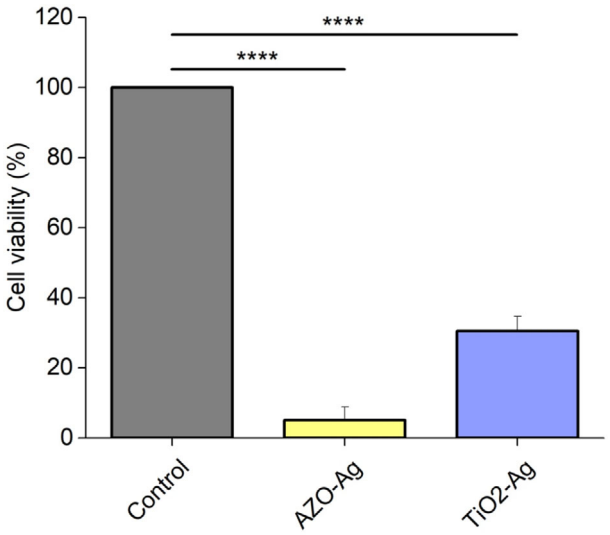

Figure 8. Cytotoxic effect of AZO-Ag and TiO_2-Ag coated surfaces on murine embryonic fibroblasts (MEFs) cells with respect to the uncoated surface. Cell viability performed by MTT assay on MEF at 24 h post treatment. ****$p < 0.0001$.

Anyhow, such toxicity detected on the tested eukaryotic cell line indicates the possible occurrence of secondary effects/side effects of the coatings, i.e., an undesired potential hazard for human cells besides the intended antimicrobial effects. For this reason, in a precautionary view, AZO-Ag and TiO_2-Ag coatings here deposited could be preferably recommended for applications where the possible impact on the human organism is less critical, like for treatment of objects and surfaces in general rather than for biomedical implants. On the other hand, it must be underlined that in the MTT assays used for cytotoxic evaluation the mammalian cells are growing in contact with the coatings, which is not the real situation usually happening in most of the final usages of the treated surfaces. Therefore, the toxicity resulting from these analyses can be considered as an overestimation of real toxicity in the common practical applications of such surface treatments. Indeed, as an example of a possible practical usage in food packaging applications, from a rough estimation of the amount of coating material deposited on the plastic surface we have a load of Ag, AZO or TiO_2 ranging from a few μg cm^{-2} up to ≈20 μg cm^{-2} at the most, that is lower than the safety maximum migration limits indicated in regulations for food contact materials,[49] thus they can be reasonably assumed as safe for such application. Nevertheless, further optimization of the coatings could be still pursued with the aim of decreasing their potential eukaryotic cytotoxicity while keeping strong and broad-range antimicrobial efficacy.

3. Conclusion

Contrasting the massive spread of infections, diseases, and deaths connected with pathogenic bacteria, fungi, and viruses is a paramount challenge for global health nowadays. The ever-increasing antimicrobial resistance and the extremely common pathway for transmission of pathogens through contaminated surfaces call for novel antimicrobial agents and effective

surface treatments. To this aim, here we have developed two nanostructured coatings (AZO-Ag and TiO_2-Ag) deposited on plastic surfaces and tested them against various critical pathogens, including high-priority Gram+ and Gram- bacteria (susceptible and resistant strains), *C. albicans* yeast, and H1N1 influenza virus. Specifically, to our knowledge, here for the first time the AZO-Ag material has been tested as antiviral agent and as surface coating against fungi and antimicrobial resistant bacterial strains. Both coatings demonstrated good antimicrobial activity, with a reduction of the bacterial population on the coated surfaces up to 99% for some strains and of the viral load up to ≈98% with respect to the uncoated control surfaces, indicating a great potential for their use on commonly touched surfaces. On the other hand, significant cytotoxicity to a tested mammalian cell line has been detected, likely due to the Ag content, recommending some caution for the use in medical applications and suggesting further optimization of the coating properties and a more extended evaluation of their potential toxicity.

The multi-assay approach here employed for evaluating the antimicrobial efficacy allowed us to derive information on the influence of direct-contact versus indirect modes of action of the tested coatings, so that indirect mechanisms resulted very relevant in both coatings, especially in TiO_2-Ag. Direct-contact ones seemed to have higher effect in AZO-Ag with respect to TiO_2-Ag against sensitive bacterial strains. Among the different possible mechanisms, ROS-mediated killing resulted as a dominant antimicrobial pathway for *K. pneumoniae* and *C. albicans*, whereas *S. aureus* appeared to evade oxidative stress, requiring different mechanisms of inactivation like membrane disruption or toxicity induced by nanoparticles and/or metal ions released from the coatings, for which additional analyses should be conducted. This species-dependent response should be considered when designing antimicrobial nanostructured surfaces for different applications.

As another important result, apart from inspecting the effectiveness of the coatings themselves, the comparison of the results coming from the different antimicrobial tests demonstrated the criticality in using one method rather than another, since different methods can produce different values of the efficacy for the same coating, depending on the prevalence of direct or indirect mechanisms of action. As consequence, it is important to be aware that the use of a single method to estimate the effectiveness of a coating could provide only a partial evaluation of the antimicrobial action. Finally, the analysis of the differences found in the multiple antimicrobial tests and the consequent considerations allow this study to draw some general guidelines for the proper selection of the coatings and of the antimicrobial tests, which can be shortly summarized as follows:

1) Whether possible, use multiple types of antimicrobial tests with prominence of direct-contact modes (e.g., live/dead fluorescence assay and SEM inspection) and indirect modes (e.g., CFU test) for a correct assessment of the coating efficacy, so to avoid deriving incomplete information.
2) If not possible, then preferably choose a test that is capable to achieve information related to the main mode of action (direct or indirect) expected in the final application.
3) Select a material (or a combination of materials) whose main mechanisms of action (direct or indirect) are congruent with the expected final use.

4. Experimental Section

Coating Deposition: All AZO-Ag and TiO_2-Ag coatings were deposited on 13mm-diameter polyester disks (Thermo Scientific Nunc Thermanox coverslips). AZO-Ag nanostructured films with an AZO thickness of 30 nm and a Ag nominal thickness of ≈6 nm (corresponding to Ag load of ≈5 μg cm^{-2}) were grown at room temperature by RF magnetron sputtering of a $ZnO:Al_2O_3$ target (composition 98:2 wt.%, purity 99.999%) and a Ag target (purity 99.99%), with similar experimental details previously reported.[18,30] The TiO_2-Ag films were obtained by supersonic cluster beam deposition (SCBD), a bottom-up physical approach to NP synthesis which relies on the plasma ablation of a target rod of the desired material to produce nanostructured films.[22,23] Here, a 99.99% purity Ag/Ti rod with a 50–50 Ag-Ti wt.% (HMW Hauner GmbH) was employed as the starting material to obtain 50 nm thick films at room temperature. It is important to stress that these SCBD-grown films have a porosity (presence of voids inside the film) up to 30%,[50] thus leading to an equivalent film thickness of 35 nm. Moreover, the Ag fraction in the film is ≈15% of the content of a pure Ag film with the same thickness,[50] thus corresponding to an Ag load of 5.5 μg cm^{-2}, comparable to that of the AZO-Ag film.

Morphological and Compositional Analyses: Field emission-gun scanning electron microscopy (FEG-SEM) and energy-dispersive X-ray spectroscopy (EDS) analyses of the samples were conducted using a ΣIGMA FEG-SEM microscope (ZEISS NTS Gmbh, Oberkochen, Germany). FEG-SEM micrographs were captured in secondary electrons mode at an acceleration voltage of 8 kV. For each sample the micrographs were acquired at magnifications ranging from 50.000× to 200.000×.

EDS surface compositional analysis was performed with an acceleration voltage of 15 kV. Immediately before sample analysis, the EDS instrument was calibrated by measuring the spectrum of a standard sample of metallic cobalt as suggested by the instrument manufacturer. Four randomly selected fields were acquired at 10.000× magnification in full-frame mode using an acquisition time of 40 s. Each field represented an interaction volume from an area of 15 μm × 15 μm and a depth of ≈1 μm. The composition and relative stoichiometry of the TiO_2-Ag films were also determined by XPS in refs. [22,50].

Antimicrobial Tests: The antimicrobial action of the AZO-Ag and TiO_2-Ag coatings on polyester disks was assessed against 6 pathogenic species, briefly: 4 bacterial strains (Gram-negative and Gram-positive, each with a susceptible and an antibiotic-resistant strain), 1 yeast, 1 virus. Furthermore, to evaluate the influence of direct-contact and non-contact antimicrobial mechanisms against the sessile and planktonic bacterial forms, two different methods were employed for measuring the antimicrobial response against the bacterial strains, namely the Colony Forming Unit (CFU) test and the LIVE/DEAD fluorescent assay, supported by SEM inspections of the specimen surfaces after the antibacterial tests.

Bacterial, Fungal, and Viral Pathogens Species: Two bacterial species were included as representative of gram-negative and gram-positive bacterial pathogens: *Klebsiella pneumoniae* and *Staphylococcus aureus*.[51] Two strains per species were included to represent both wild-type (susceptible) and AMR phenotypes. The selected wild-type strains were *K. pneumoniae* ATCC 700603 and *S. aureus* ATCC 29213, susceptible to Carbapenems and Methicillin, respectively. The AMR strains were derived from clinical positive blood cultures and were identified through Bruker biotyper MALDI-TOF mass spectrometer (Bruker Daltonics, Bremen, Germany). To assess antibiotic susceptibility, semi-automated microbroth dilutions were performed via VITEK2 instrument (bioMérieux, Marcy l'Étoile, France). The two resistant strains resulted as a Carbapenem-resistant *K. pneumoniae* and a Methicillin-resistant *S. aureus* (MRSA), according to EUCAST breakpoint v14.0.[52] As representative of fungal opportunistic pathogens, a clinical strain of *Candida albicans* was selected. The yeast strain was isolated from a positive blood culture and was identified via MALDI-TOF. Finally,

the Influenza H1N1 strain was derived from a bronchoalveolar lavage, was identified through BIOFIRE FilmArray Respiratory Panel (bioMérieux), and was used to assess antiviral action of coatings.

Colony Forming Unit (CFU) Test: *K. pneumoniae* strains were grown on Luria–Bertani (LB) Broth (25 g L^{-1}) (Condalab cat.1551 Laboratories CONDA, Espana) at 37 °C, *S. aureus* strains were grown on Nutrient Broth (NB) (8 g L^{-1}) (Panreac Applichem, Germany, cat. 413793.1210) at 37 °C, and *C. albicans* was grown on Sabouraud Broth (Sigma–Aldrich, Italy, cat. 1.08339) at 35 °C. CFU tests were performed on broth/Agar (LP0011 Oxoid) 15 g L^{-1} plates. To set up the best interval times showing an exponential growth phase, growth curve experiments were performed for all bacterial and yeast strains. Colony forming unit test was performed as follows: O/N cultures of bacteria were diluted 1:200 in appropriate broth and grown until reaching an absorbance value of 0.02 at $\lambda = 600$ nm, indicating a bacterial concentration of $\approx 2 \times 10^3$ colony forming units/mL (CFU mL^{-1}), and tested at T0, 1.5 h, 3 h and, only for the resistant strains, also at 4.5 h. *C. albicans* O/N culture, showing a slower growth, was diluted 1:10 in Sabouraud broth and directly tested at 0, 4, and 6 h. Briefly, 0.5 mL of suspension were poured in a 24-well plate in the presence of *i)* uncoated disk, *ii)* AZO-Ag coated and *iii)* TiO_2-Ag coated disks, and incubated under constant agitation at 150 rpm. At the indicated time points, spots of 10 µl of scalar dilutions from 10^{-8} to 10^{-2} of the bacterial suspensions, were poured on broth/Agar plates in triplicate, and further 100 µl of diluted bacterial suspensions (10^{-4} and 10^{-5}) were plated on 100 mm diameter plates for more accurate colonies count. Plates were incubated O/N for CFU count. The experiment was repeated three times for each strain, and the concentration of CFU mL^{-1} was quantified for each condition.

SEM Antimicrobial Evaluation: Bacterial and fungal inocula, adjusted to a turbidity equivalent to the 1 McFarland standard ($\approx 3 \times 10^8$ CFU mL^{-1}) in 0.9% sodium chloride saline solution, were prepared using the Densicheck Plus (bioMérieux). One milliliter of each inoculum was applied to tested surfaces in a 24-well plate (Corning Incorporated, NY, USA), which was then incubated at 37 °C with 5% CO_2 for 4 h. After incubation, the samples were dehydrated via immersion in an increasing ethanol concentration, from 30% to 100%, with a multi-step procedure of 10 min each. Successively, they were gold-metallized using a High Resolution Sputter Coater AGB7234 (Agar Scientific, Stansted, UK). The morphology of the microbe cells on the sample surfaces was observed with Supra25 SEM microscope (Zeiss, Oberkochen, Germany). Representative micrographs were acquired in secondary electrons mode at an acceleration voltage of 15 kV. For each sample at least four randomly selected fields were acquired at magnification of 15.000× for bacteria and 5.000× for *C. albicans*.

Live/Dead Fluorescence Assay: The samples were incubated with bacterial and fungal inocula as described above for the SEM antimicrobial evaluation. After incubation, to distinguish between live and dead bacterial cells, the LIVE/DEAD BacLight Bacterial Viability kit (Thermofisher Scientific, Waltham, MA, USA) was employed following the manufacturer's guidelines. Visualization of the fluorescent staining was conducted with the Cytation5 reader (Biotek, Winooski, VT, USA), using excitation wavelengths of 469 and 586 nm, and emission wavelengths of 525 and 647 nm for the green and red channels, respectively. Quantitative analysis of the fluorescence emission was performed using ImageJ Fiji Software (Version 1.53c).

Quantification of Reactive Oxygen Species (ROS): The induction of oxidative stress by nanostructured surfaces of AZO-Ag and TiO_2-Ag toward bacterial and fungal cells was evaluated using the DCFDA/H2DCFDA cellular ROS assay kit (Abcam, Cambridge, United Kingdom). *K. Pneumoniae* (5×10^8 CFU mL^{-1}), *S. aureus* (5×10^8 CFU mL^{-1}), and *C. albicans* (5×10^6 CFU mL^{-1}) cells in saline solution were placed in contact with coated and uncoated control surfaces in a 24-well plate for 24 h. Subsequently, bacterial and fungal cells were collected by centrifugation, and the DCFDA staining was performed according to manufacturer's instructions. Fluorescent quantification was conducted in a 96-wells black plate optimized for fluorescence contexts (Nunc, Roskilde, Denmark) using a Cytation5 multimode reader (Biotek). The fluorescent readings were performed with excitation/emission wavelength at 485 nm/535 nm. The absorbance readings were performed with the same instrument at 600 nm to normalize the fluorescence data based on cellular abundance.

Virucidal Activity of Surfaces Against H1N1 Influenza Virus in MDCK-SIAT1 Cells: MDCK-SIAT1 cells (ECACC No. 05071502[53]) were grown in DMEM medium high glucose, w/o L-Glutamine, (Thermo Fisher Scientific) supplemented with 10% FBS (Gibco, Life Technologies Corporation, NY, USA), 1% L-glutamine (Sigma–Aldrich, St. Louis, MO, USA), 1% Penicillin/Streptomycin (Gibco, Life Technologies Corporation).

A standardized volume of 250 µl of H1N1 virus was applied to each surface (uncoated, AZO-Ag coated and TiO_2-Ag coated disks) and incubated for 2 h. The suspension was used to infect monolayers of MDCK-SIAT1 cells grown on plastic discs for subsequent immunofluorescence analysis. Infection was carried out at 37 °C for 3 h in medium containing TPCK-trypsin. After 5 days of incubation, RNA was extracted from the cells (EZ1, QIAGEN, Hilden, Germany) and purified with RNeasy Mini Kit (QIAGEN). The RNA concentration was measured at 280 nm with VarioScan (Thermo Scientific Varioskan LUX multimode microplate reader). Purified RNA was reverse transcribed into cDNA using the SuperScript III First-Strand Synthesis System (Invitrogen, Life Technologies), followed by CFX Opus 96 real-time PCR (Bio-rad, Hercules, CA, USA) to assess viral M protein expression. The following primers were used according to WHO guidelines.[54]

Primer Forward: ATGAGYCTTYTAACCGAGGTCGAAACG (Tm 65 °C).

Primer Reverse: TGGACAAANCGTCTACGCTGCAG (Tm 63,3 °C).

The experiment evaluates the reduction of M protein expression in H1N1-infected cells after surface treatment. As stated in the 7th version of "WHO information for molecular diagnosis of influenza virus",[54] matrix (M) gene amplified with indicated primers generates a 244 bp PCR product that is widely effective for the identification of influenza type A viruses in human specimens.

Immunofluorescence was performed using an anti-HA antibody to detect the viral haemagglutinin (HA) protein. The cell monolayer was fixed in methanol/acetone (Carlo Erba reagents, Milian, Italy), permeabilized with Triton X-100 (Bio-rad), and then incubated with a 1:250 diluted primary antibody (MA 54239 Rabbit, ThermoFisher Scientific) specific for exposed HA protein of H1N1. After rinsing steps, cell monolayer was exposed to a 1:4000 diluted secondary antibody conjugated with FITC (A 10530, ThermoFisher Scientific). The nuclei were stained with DAPI (ThermoFisher Scientific), and the fluorescence was visualized using Eclipse Nikon confocal microscope (Nikon Europe B.V, Amstelveen, Netherlands). The experiment included: positive control (virus), negative control (medium only), specificity control (secondary antibody exposition without primary antibody).

Assessment of Microbial Reduction and Antimicrobial Activity: To compare the results obtained by the different methods employed for the evaluation of the antimicrobial action of the samples, the microbial reduction *R* induced by the coated surfaces with respect to the uncoated control surfaces can be introduced as an estimation of the coating antimicrobial efficiency:

$$R\,(\%) = \left(1 - \frac{T}{C}\right) \times 100 \quad (1)$$

where:

T = concentration of viable microorganisms detected on the coated Test surfaces;

C = concentration of viable microorganisms detected on the uncoated Control disks.

More specifically, referring to each method used in our work, *T* and *C* are intended as follows:

- In live/dead assays, the fluorescence intensity of live cells detected after 4 h on the coated surface (*T*) and on the control substrate (*C*).
- In CFU mL^{-1} experiments, the microbial concentration measured for the coated surface (*T*) and the control substrate (*C*), detected at 3 h for bacteria and 4 h for yeast.
- In real-time PCR measurements, the viral load expressed as $2^{-\Delta\Delta Ct}$ measured on the coated surface (*T*) and on the infected control substrate (*C*).

As an equivalent way to express the coating effectiveness in reducing the microbial population with respect to the uncoated surface, we can also

represent the coating efficiency in the Logarithmic form, analogously to the antimicrobial activity defined in the ISO standards for bacteria and viruses,[55,56] introducing the antimicrobial activity (here denoted as *A*), expressed as:

$$A = (U_t - U_0) - (S_t - U_0) = U_t - S_t = Log\frac{C}{T} \quad (2)$$

where:

U_0 = Logarithm of the initial concentration of viable microorganisms;

$U_t = Log\ C$ = Logarithm of the concentration of viable microorganisms detected on the uncoated control surface at the considered time period *t* mentioned above;

$S_t = Log\ T$ = Logarithm of the concentration of viable microorganisms detected on the coated specimen surface at the same time period *t*.

Cytotoxicity on Mammalian Cells: To test if the coated disks had a toxic effect on mammalian cells, we performed the MTT cell viability test (Sigma–Aldrich) on murine embryonic fibroblasts (MEF) (RRID:CVCL_9092, immortalized with 3T3 method as purchased from HMGBiotech, Milan, Italy) grown in D-MEM (EuroClone, Milan, Italy cat. ECB750) + 10%FCS (EuroClone) at 24 h. MEF culture at ≈60% confluence were detached, washed and counted. A number of 2×10^4 cells well^{-1} in 0,5 mL of media was poured in 24-well plates containing the disks coated with AZO-Ag, TiO_2-Ag or uncoated control disks. Cells were grown at 37 °C and 5%CO_2 for 24 h before performing the viability MTT test. After 24 h of cells growth on the disks, the exhausted media was substituted by 500 µl of fresh media containing 50 µl of a 5 mg mL^{-1} MTT solution and incubated at 37 °C for 60 min. The MTT containing media was substituted by 500 µl of solubilization solution (11 g SDS in 50 mL of 0.02 M HCl and 50 mL isopropyl alcohol) for 15 min. 200 µl of solution from wells were poured in a 96-well plate and read at λ = 560 nm by Promega Glomax Spectrophotometer.

Statistical Analysis: Prior to statistical analysis, data were preprocessed as follows. Fluorescent intensity values were expressed as percentages, calculated by dividing the single-channel intensity by the total fluorescence emission, using Fiji (ImageJ). Real-time PCR results were expressed as $2^{-\Delta\Delta Ct}$. Quantification of reactive oxygen species (ROS) was determined as the ratio between fluorescence emission (at wavelengths specified by the manufacturer) and absorbance at 600 nm, the latter used to normalize for sample load after 24 h incubation with tested surfaces. Cell viability was expressed as percentages, calculated as follow (%) = [(Absorbance sample − Absorbance blank)/(Absorbance control − Absorbance blank)] × 100.

For the live/dead fluorescent assay, real-time PCR, viral immunofluorescence, ROS quantification, and cytotoxicity, upon confirmation of normal distribution, statistical comparisons were performed using a one-way ANOVA test (two-sided). For CFU testing during time, comparisons among groups in different time-points were performed using the two-way ANOVA test (two-sided). All experiments were repeated three times, and data were given as mean ± standard deviation (SD). All statistical analyses were performed with GraphPad InStat software v10 (GraphPad Software, San Diego, CA, USA). Differences were noted as significant * $p < 0.05$, ** $p < 0.01$, *** $p < 0.001$, ****$p < 0.0001$.

Acknowledgements

D.S. and R.V. contributed equally to this work. The authors would like to acknowledge the contribution of 3D-Bioprinting Core Facilty G-STeP of the Fondazione Policlinico Universitario "A. Gemelli" IRCCS for sample processing. The authors are grateful to Alberto Augello for his valuable technical support. ENEA (Italian National Agency for New Technologies, Energy and Sustainable Economic Development) activities in this work were funded through project ECS 0000024 Rome Technopole, CUP B83C22002820006, National Recovery and Resilience Plan (NRRP), Mission 4, Component 2 Investment 1.5, funded from the European Union – NextGenerationEU. S.O. was supported by the European Union, Next Generation EU Supersonic Cluster beam synthesis of Innovative TRansition metal Oxides PHotoelectrodes for HYdrogen production (SCI-TROPHY), call MUR PRIN 2022, Prot. 2022474YE8, CUP J53D23007340008. F.B. is grateful for EU funding within the MUR PNRR Extended Partnership Initiative on Emerging Infectious Diseases (Project no. PE00000007, INF-ACT). C.F. acknowledges the Italian Ministry of University and Research (Project funded under the National Recovery and Resilience Plan (NRRP), funded by the European Union - NextGenerationEU - Mission 4 Component 1 Investment 3.3 - Call for tender No. 117 of 02/03/2023.

Open access publishing facilitated by ENEA Agenzia Nazionale per Le Nuove Tecnologie l'Energia e lo Sviluppo Economico Sostenibile, as part of the Wiley - CRUI-CARE agreement.

Conflict of Interest

The authors declare no conflict of interest.

Data Availability Statement

The data that support the findings of this study are available from the corresponding author upon reasonable request.

Keywords

antibacterial, antifungal, antimicrobial mechanisms, antiviral, coatings, metal oxide, nanomaterials

Received: July 7, 2025
Revised: September 4, 2025
Published online: October 3, 2025

[1] K. S. Ikuta, L. R. Swetschinski, G. Robles Aguilar, F. Sharara, T. Mestrovic, A. P. Gray, N. Davis Weaver, E. E. Wool, C. Han, A. Gershberg Hayoon, A. Aali, S. M. Abate, M. Abbasi-Kangevari, Z. Abbasi-Kangevari, S. Abd-Elsalam, G. Abebe, A. Abedi, A. P. Abhari, H. Abidi, R. G. Aboagye, A. Absalan, H. Abubaker Ali, J. M. Acuna, T. D. Adane, I. Y. Addo, O. A. Adegboye, M. Adnan, Q. E. S. Adnani, M. S. Afzal, et al., *Lancet* **2022**, *400*, 2221.

[2] C. J. L. Murray, K. S. Ikuta, F. Sharara, L. Swetschinski, G. Robles Aguilar, A. Gray, C. Han, C. Bisignano, P. Rao, E. Wool, S. C. Johnson, A. J. Browne, M. G. Chipeta, F. Fell, S. Hackett, G. Haines-Woodhouse, B. H. Kashef Hamadani, E. A. P. Kumaran, B. McManigal, S. Achalapong, R. Agarwal, S. Akech, S. Albertson, J. Amuasi, J. Andrews, A. Aravkin, E. Ashley, F.-X. Babin, F. Bailey, et al., *Lancet* **2022**, *399*, 629.

[3] M. Naghavi, S. E. Vollset, K. S. Ikuta, L. R. Swetschinski, A. P. Gray, E. E. Wool, G. Robles Aguilar, T. Mestrovic, G. Smith, C. Han, R. L. Hsu, J. Chalek, D. T. Araki, E. Chung, C. Raggi, A. Gershberg Hayoon, N. Davis Weaver, P. A. Lindstedt, A. E. Smith, U. Altay, N. V. Bhattacharjee, K. Giannakis, F. Fell, B. McManigal, N. Ekapirat, J. A. Mendes, T. Runghien, O. Srimokla, A. Abdelkader, et al., *Lancet* **2024**, *404*, 1199.

[4] WHO Bacterial Priority Pathogens List, 2024: Bacterial Pathogens of Public Health Importance to Guide Research, Development and Strategies to Prevent and Control Antimicrobial Resistance, World Health Organization, Geneva **2024**.

[5] S.-J. Huang, Y.-H. Song, G. Lv, J.-Y. Liu, J.-T. Zhao, L.-L. Wang, M.-J. Xiang, *Front. Microbiol.* **2025**, *16*, 1550894.

[6] WHO Fungal Priority Pathogens List to Guide Research, Development and Public Health Action, World Health Organization, Geneva **2022**.

[7] G. Ramage, J. P. Martínez, J. L. López-Ribot, *FEMS Yeast Res.* **2006**, *6*, 979.
[8] https://www.who.int/news-room/fact-sheets/detail/influenza-(seasonal) (accessed: September 2025).
[9] P. Suárez-Sánchez, J. Majuelos-Melguizo, M. Hinojosa-Campos, B. Podmore, I. Gillespie, J. Han, R. Sloot, D. Christensen, *Influenza Other Respi. Viruses* **2025**, *19*, 70073.
[10] A. Kramer, F. Lexow, A. Bludau, A. M. Köster, M. Misailovski, U. Seifert, M. Eggers, W. Rutala, S. J. Dancer, S. Scheithauer, *Clin. Microbiol. Rev.* **2024**, *37*, 00186.
[11] M. H. Y. Leung, X. Tong, P. K. H. Lee, *Compr. Biotechnol.* **2019**, *6*, 96.
[12] P. Makvandi, C. yu Wang, E. N. Zare, A. Borzacchiello, L. na Niu, F. R. Tay, *Adv. Funct. Mater.* **2020**, *30*, 1910021.
[13] J. Butler, R. D. Handy, M. Upton, A. Besinis, *ACS Nano* **2023**, *17*, 7064.
[14] S. Jabeen, E. Veg, M. I. Ahmad, S. Bala, T. Khan, *ChemistrySelect* **2025**, *10*, 202500080.
[15] K. Wieczerzak, F. F. Klimashin, A. Sharma, S. Altenried, K. Maniura-Weber, Q. Ren, J. Michler, *ACS Appl. Mater. Interfaces* **2024**, *16*, 60018.
[16] F. Sahin, A. Camdal, G. Demirel Sahin, A. Ceylan, M. Ruzi, M. S. Onses, *ACS Appl. Mater. Interfaces* **2023**, *15*, 11563.
[17] D. Valerini, L. Tammaro, R. Vitali, G. Guillot, A. Rinaldi, *Coatings* **2021**, *11*, 345.
[18] N. Fiaschini, C. Giuliani, R. Vitali, L. Tammaro, D. Valerini, A. Rinaldi, *Nanomaterials* **2022**, *12*, 3962.
[19] E. Cavaliere, S. De Cesari, G. Landini, E. Riccobono, L. Pallecchi, G. M. Rossolini, L. Gavioli, *Nanomed. Nanotechnol., Biol. Med.* **2015**, *11*, 1417.
[20] D. Valerini, L. Tammaro, F. Di Benedetto, G. Vigliotta, L. Capodieci, R. Terzi, A. Rizzo, *Thin Solid Films* **2018**, *645*, 187.
[21] D. Valerini, L. Tammaro, F. Villani, A. Rizzo, I. Caputo, G. Paolella, G. Vigliotta, *J. Mater. Sci.* **2020**, *55*, 4830.
[22] G. Benetti, E. Cavaliere, A. Canteri, G. Landini, G. M. Rossolini, L. Pallecchi, M. Chiodi, M. J. Van Bael, N. Winckelmans, S. Bals, L. Gavioli, *APL Mater.* **2017**, *5*, 036105.
[23] G. Benetti, E. Cavaliere, F. Banfi, L. Gavioli, *Materials* **2020**, *13*, 784.
[24] C. Manoharan, G. Pavithra, M. Bououdina, S. Dhanapandian, P. Dhamodharan, *Appl. Nanosci.* **2016**, *6*, 815.
[25] H. J. Choi, S. V. N. Pammi, B. J. Park, J. H. Eom, H. An, H. Y. Kim, M. Kim, D. Seol, Y. Kim, S. G. Yoon, *J. Alloys Compd.* **2017**, *719*, 271.
[26] J. H. Eom, T. Y. Cho, S. K. Cho, *Appl. Surf. Sci.* **2023**, *638*, 158011.
[27] Q. Wang, Z. Tang, R. Herout, C. Liu, K. Yu, D. Lange, R. Godin, J. N. Kizhakkedathu, T. Troczynski, R. Wang, *Surf. Interfaces* **2024**, *45*, 103856.
[28] R. G. S. V. Prasad, D. Basavaraju, K. N. Rao, C. S. Naveen, J. Endrino, A. R. Phani, in 2011 Int. Conf. Nanosci. Technol. Soc. Implic. NSTSI11, **2011**, pp. 1–6.
[29] B. Moongraksathum, M.-Y. Chien, Y.-W. Chen, *J. Nanosci. Nanotechnol.* **2019**, *19*, 7356.
[30] D. Valerini, L. Tammaro, G. Vigliotta, E. Picariello, F. Banfi, E. Cavaliere, L. Ciambriello, L. Gavioli, *Coatings* **2020**, *10*, 1238.
[31] S. H. Zyoud, A. Ashames, A. H. Zyoud, A. R. Prasad, C. A. C. Abdullah, S. H. Zyoud, I. S. Yahia, G. N. Makhadmeh, A. Khalid, N. Qamhieh, H. Y. Zahran, S. Muhammad, M. S. Abdel-wahab, *Mater. Sci. Eng. B* **2024**, *309*, 117649.
[32] M. K. L. N. Sikosana, A. Ruland, C. Werner, L. D. Renner, *Appl. Environ. Microbiol.* **2022**, *88*, 02241.
[33] P. D. Rakowska, M. Tiddia, N. Faruqui, C. Bankier, Y. Pei, A. J. Pollard, J. Zhang, I. S. Gilmore, *Commun. Mater.* **2021**, *2*, 53.
[34] R. Kaur, S. Liu, *Prog. Surf. Sci.* **2016**, *91*, 136.
[35] E. Sharifikolouei, Z. Najmi, A. Cochis, A. C. Scalia, M. Aliabadi, S. Perero, L. Rimondini, *Mater. Today Bio* **2021**, *12*, 100148.
[36] J. Wu, H. Wei, Y. Wei, T. Deng, Y. Wang, Y. Qiu, Y. Zhang, *ACS Appl. Mater. Interfaces* **2024**, *16*, 11194.
[37] S. Schienle, A. Al-Ahmad, R. J. Kohal, F. Bernsmann, E. Adolfsson, L. Montanaro, P. Palmero, T. Fürderer, J. Chevalier, E. Hellwig, L. Karygianni, *Clin. Oral Investig.* **2016**, *20*, 1719.
[38] E. O. Ogunsona, R. Muthuraj, E. Ojogbo, O. Valerio, T. H. Mekonnen, *Appl. Mater. Today* **2020**, *18*, 100473.
[39] C. Kate, C. Graham, J. Ing-Marie, T. Andrej, K.-K. F. John, M. J. James, F. J. Simon, *J. Bacteriol.* **2007**, *189*, 1025.
[40] N. Kashef, M. R. Hamblin, *Drug Resist. Updat.* **2017**, *31*, 31.
[41] R. Gaupp, N. Ledala, G. A. Somerville, *Front. Cell. Infect. Microbiol.* **2012**, *2*, 33.
[42] M. M. El-Kady, I. Ansari, C. Arora, N. Rai, S. Soni, D. K. Verma, P. Singh, A. E. D. Mahmoud, *J. Mol. Liq.* **2023**, *370*, 121046.
[43] A. B. Sengul, E. Asmatulu, *Environ. Chem. Lett.* **2020**, *18*, 1659.
[44] J. Zhang, F. Wang, S. S. K. Yalamarty, N. Filipczak, Y. Jin, X. Li, *Int. J. Nanomed.* **2022**, *17*, 1851.
[45] H. Liang, H. Wang, X. Sun, W. Xu, N. Meng, N. Zhou, *Appl. Clay Sci.* **2023**, *244*, 107112.
[46] O. Bondarenko, K. Juganson, A. Ivask, K. Kasemets, M. Mortimer, A. Kahru, *Arch. Toxicol.* **2013**, *87*, 1181.
[47] M. Asif, M. Fakhar-e-Alam, M. Tahir, F. Jamil, H. Sardar, J. Rehman, K. A. Dahlous, *Pharmaceuticals* **2024**, *17*, 1216.
[48] V. Saxena, P. Chandra, L. M. Pandey, *Appl. Nanosci.* **2018**, *8*, 1925.
[49] European Commission, Commission Regulation (EU) No 10/2011 of 14 January 2011 on Plastic Materials and Articles Intended to Come into Contact with Food. Consolidated Text Version of 16.03.2025, **2025**. Document no. 02011R0010-20250316.
[50] E. Cavaliere, G. Benetti, M. Van Bael, N. Winckelmans, S. Bals, L. Gavioli, *Nanomaterials* **2017**, *7*, 442.
[51] W. R. Miller, C. A. Arias, *Nat. Rev. Microbiol.* **2024**, *22*, 598.
[52] "EUCAST. Breakpoint Tables for Interpretation of MICs and Zone Diameters, Version 14.0, 2024", http://www.eucast.org, (accessed: September 2025).
[53] https://www.culturecollections.org.uk/nop/product/mdck-siat1 (accessed: September 2025).
[54] "WHO information for molecular diagnosis of influenza virus," 2021, https://www.who.int/teams/global-influenza-programme/laboratory-network/quality-assurance/eqa-project/information-for-molecular-diagnosis-of-influenza-virus, (accessed: September 2025).
[55] ISO 22196:2011– Measurement of Antibacterial Activity on Plastics and Other Non-Porous Surfaces (Edition 2, 2011), **2011**.
[56] ISO 21702:2019 – Measurement of Antiviral Activity on Plastics and Other Non-Porous Surfaces (Edition 1, 2019), **2019**.